Electronic Supplementary Material (ESI) for Analyst.

Supplementary Information

Multiplexing Potential of NIR Resonant and Non-Resonant Raman Reporters for Bio-Imaging Applications

Olga E. Eremina,[†,‡] Sarah Schaefer,[†,‡] Alexander T. Czaja,[†,‡] Samer Awad,[†,‡]

Matthew A. Lim,[†,‡] Cristina Zavaleta[†,‡,*]

[†] *Department of Biomedical Engineering, University of Southern California, 3650 McClintock Ave, Los Angeles, CA 90089, United States.*

[‡] *Michelson Center for Convergent Bioscience, University of Southern California, 1002 Childs Way, Los Angeles, CA 90089, United States.*

Corresponding Author
* Cristina Zavaleta, czavalet@usc.edu

Table of Contents

1. SERRS Spectral Signatures.....S2
2. Correlation Matrices and Condition Numbers.....S12
3. Experimental Design S14
4. References S16

1. SERRS Spectral Signatures

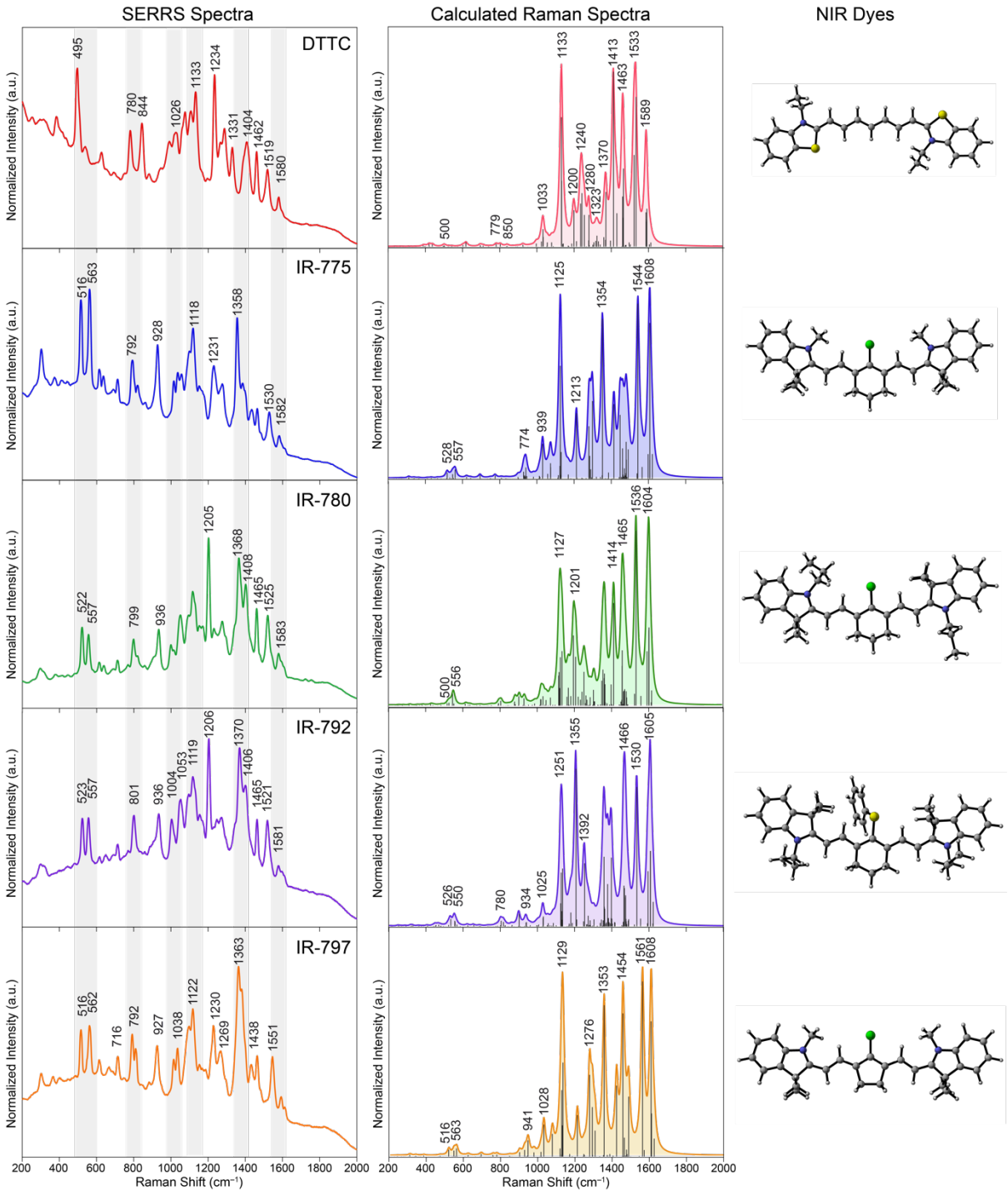

Figure S1. Experimental SERRS spectra of AuNPs labeled with one of the following NIR dyes: DTTC, IR-775, IR-780, IR-792, or IR-797; DFT-calculated Raman spectra at B3LYP/6-31++G(d,p) Raman spectrum; chemical structures of the heptamethine cyanine NIR-resonant Raman reporters that were embedded in the NIR-SERRS nanoparticles.

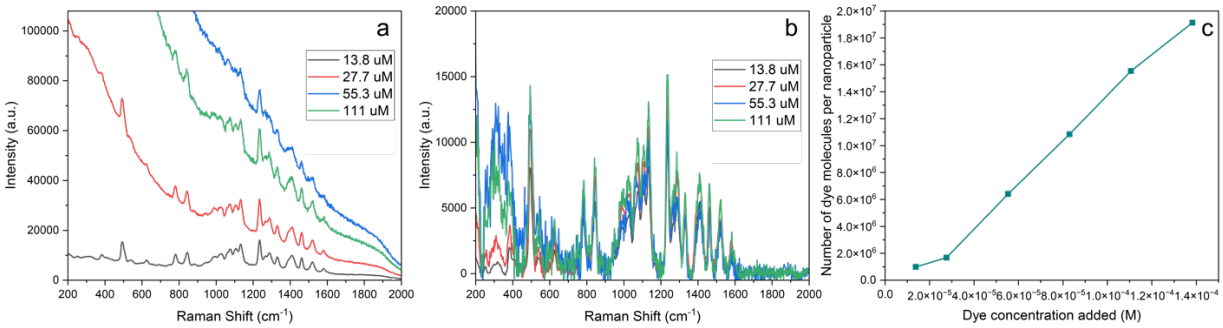

Figure S2. Experimental raw (a) and baseline-subtracted (b) SERRS spectra of AuNPs reacted with different concentrations of **DTTC**: 13.8, 27.7, 55.3, and 111 µM. Raman spectra were acquired for 5.7 pM nanoparticle suspension using 2.5% neutral density filter, 0.5 s acquisition time. A concentration of 13.8 µM DTTC was chosen for the further multiplexing experiments. (c) Loading efficiency of DTTC dye on the AuNP surface calculated based on UV-vis absorbance of supernatants from washes at 764 nm.

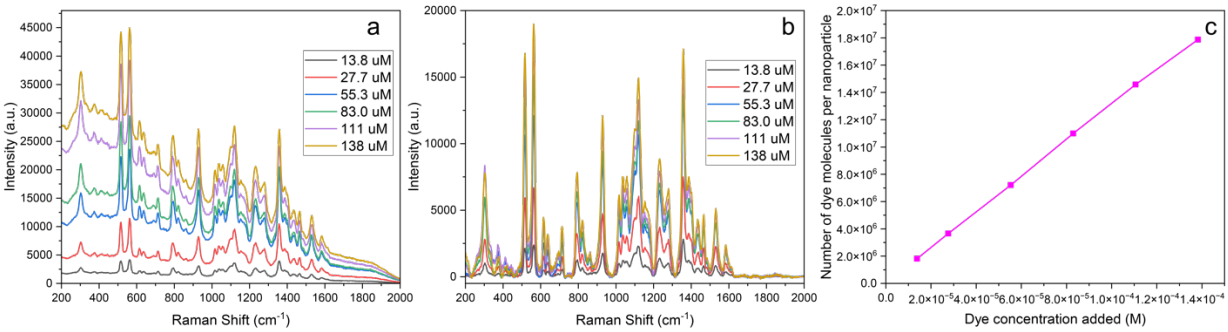

Figure S3. Experimental raw (a) and baseline-subtracted (b) SERRS spectra of AuNPs reacted with different concentrations of **IR-775**: 13.8, 27.7, 55.3, 83.0, 111, and 138 µM. Raman spectra were acquired for 5.7 pM nanoparticle suspension using 2.5% neutral density filter, 0.5 s acquisition time. A concentration of 55.3 µM IR-775 was chosen for the further multiplexing experiments. (c) Loading efficiency of IR-775 dye on the AuNP surface calculated based on UV-vis absorbance of supernatants from washes at 779 nm.

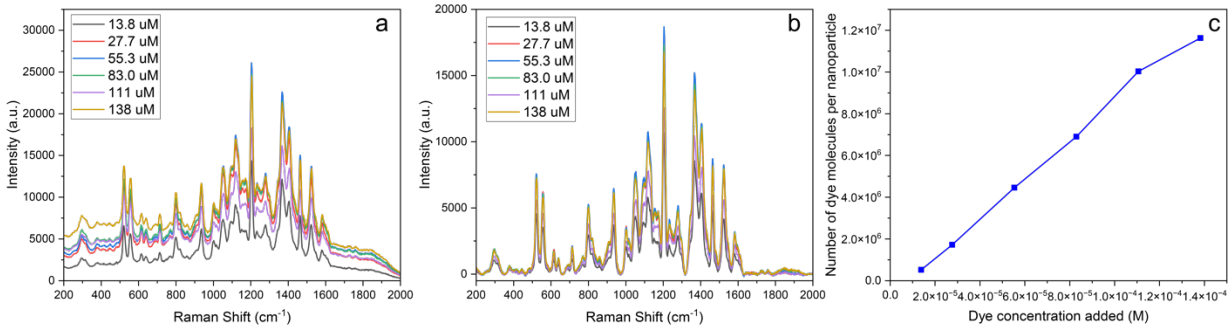

Figure S4. Experimental raw (a) and baseline-subtracted (b) SERRS spectra of AuNPs reacted with different concentrations of **IR-780**: 13.8, 27.7, 55.3, 83.0, 111, and 138 µM.

Raman spectra were acquired for 5.7 pM nanoparticle suspension using 2.5% neutral density filter, 0.5 s acquisition time. A concentration of 55.3 µM IR-780 was chosen for the further multiplexing experiments. (c) Loading efficiency of IR-780 dye on the AuNP surface calculated based on UV-vis absorbance of supernatants from washes at 783 nm.

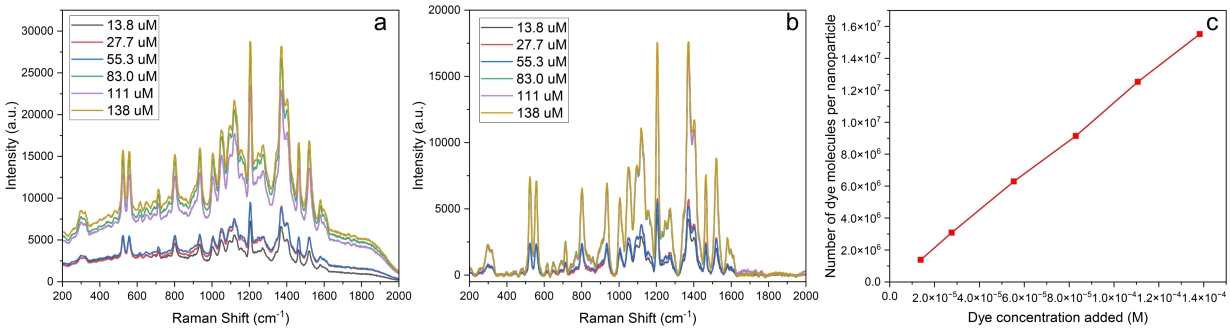

Figure S5. Experimental raw (a) and baseline-subtracted (b) SERRS spectra of AuNPs reacted with different concentrations of **IR-792**: 13.8, 27.7, 55.3, 83.0, 111, and 138 µM. Raman spectra were acquired for 5.7 pM nanoparticle suspension using 2.5% neutral density filter, 0.5 s acquisition time. A concentration of 55.3 µM IR-792 was chosen for the further multiplexing experiments. (c) Loading efficiency of IR-792 dye on the AuNP surface calculated based on UV-vis absorbance of supernatants from washes at 797 nm.

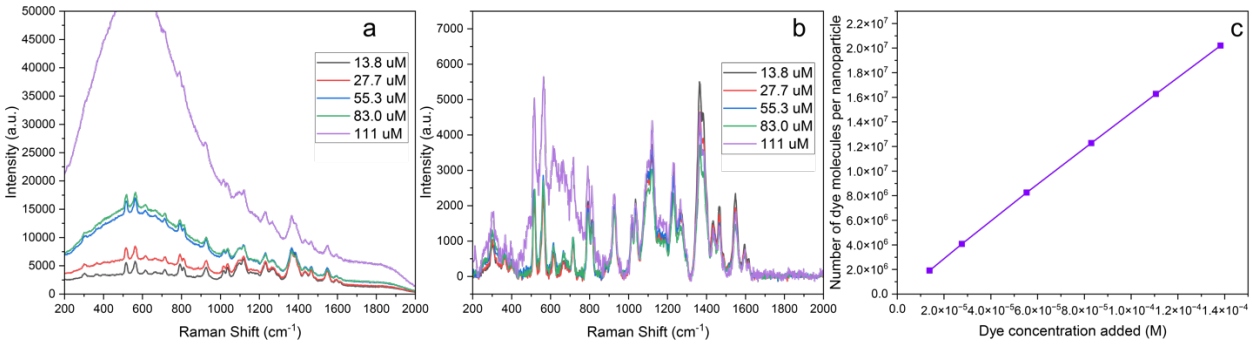

Figure S6. Experimental raw (a) and baseline-subtracted (b) SERRS spectra of AuNPs reacted with different concentrations of **IR-797**: 13.8, 27.7, 55.3, 83.0, and 111 µM. Raman spectra were acquired for 5.7 pM nanoparticle suspension using 2.5% neutral density filter, 0.5 s acquisition time. A concentration of 13.8 µM IR-797 was chosen for the further multiplexing experiments. (c) Loading efficiency of IR-797 dye on the AuNP surface calculated based on UV-vis absorbance of supernatants from washes at 804 nm.

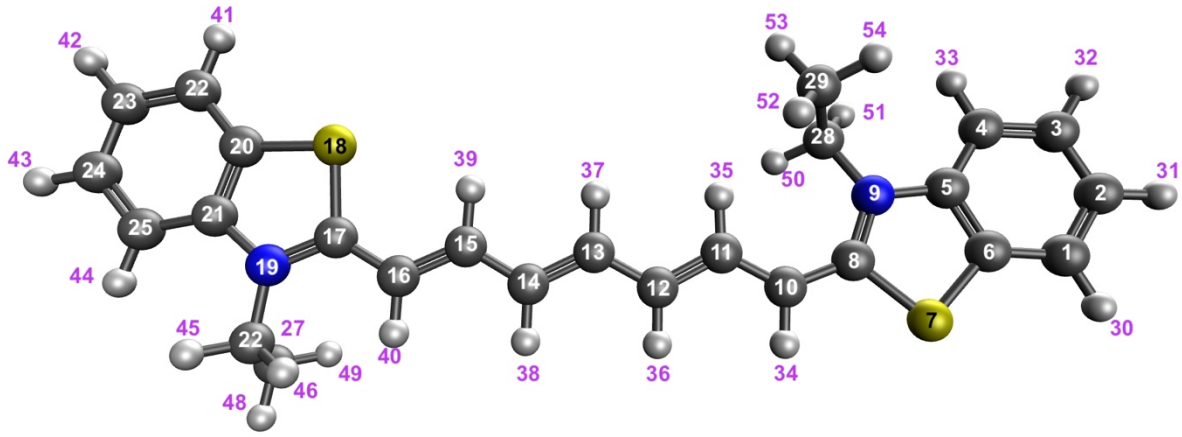

Figure S7. Chemical structure of DTTC with geometry optimized at B3LYP/6-31++G(d,p).

Table S1. Comparison of the experimental and calculated (B3LYP/6-311++G(d,p)) Raman spectra of DTTC (Figure S3) in spectral range 200 – 2000 cm^{-1}.

Raman Shift, cm^{-1}		Assignments[b]
Experimental	Calculated[a]	
495	500	$\nu(C_{20}–S_{18}–C_{17})$, $\delta(H_{45}–C_{26}–H_{46})$, $\delta(C–C)_{allyl}$
780	779	$\delta(H_{45}–C_{26}–H_{46})$, $\delta(H_{47}–C_{27}–H_{49})$
844	850	$\delta(H_{45}–C_{26}–H_{46})$, $\delta(H_{47}–C_{27}–H_{49})$, $\omega(H_{33}–C_4–C_3–H_{32})$, $\omega(H_{31}–C_2–C_1–H_{30})$
1026	1033	$\nu(C_3–C_2)$, $\delta(C_4–H_{33})$, $\delta(C_3–H_{32})$, $\delta(C_2–H_{31})$, $\delta(C_1–H_{30})$
1133	1133	$\delta(H_{45}–C_{26}–H_{46})$, $\delta(C_{25}–C_{44})$, $\delta(C_{21}–N_{19}–C_{17})$
1201	1200	$\delta(C_{15}–H_{39})$, $\delta(C_{13}–H_{37})$, $\delta(C_{11}–H_{35})$
1234	1240	$\nu(N_9–C_5)$, $\delta(C_1–H_{30})$, $\delta(C_{15}–H_{39})$, $\delta(C_{13}–H_{37})$, $\delta(C_{11}–H_{35})$
1280	1280	$\delta(C_{25}–H_{44})$, $\delta(C_{22}–H_{41})$, $\delta(H_{45}–C_{22}–H_{46})$
1331	1323	$\omega(H_{45}–C_{26}–H_{46})$, $\nu(C_{26}–N_{19})$, $\delta(C_{14}–H_{38})$, $\delta(C_{11}–H_{35})$
1372	1370	$\delta(C_{26}–H_{46})$, $\omega(H_{50}–C_{28}–H_{51})$
1404	1413	$\delta(C_{10}–H_{34})$, $\nu(C_8–N_9)$, $\delta(H_{45}–C_{26}–H_{46})$
1462	1463	$\nu(C_{21}–C_{22})$, $\delta(C_{25}–H_{44})$, $\delta(C_{24}–H_{43})$
1519	1533	$\nu(N_{19}–C_{17}–C_{16})$, $\nu(C_{15}–C_{14}–C_{13})$, $\nu(C_{11}–C_{10}–C_8)$, $\delta(H_{45}–C_{26}–H_{46})$
1580	1589	$\nu(C_4=C_5)$, $\nu(C_1=C_2)$

[a] Empirically chosen scaling factor: 0.98.

[b] ν, stretch; δ, in-plane bend; ω, wagging.

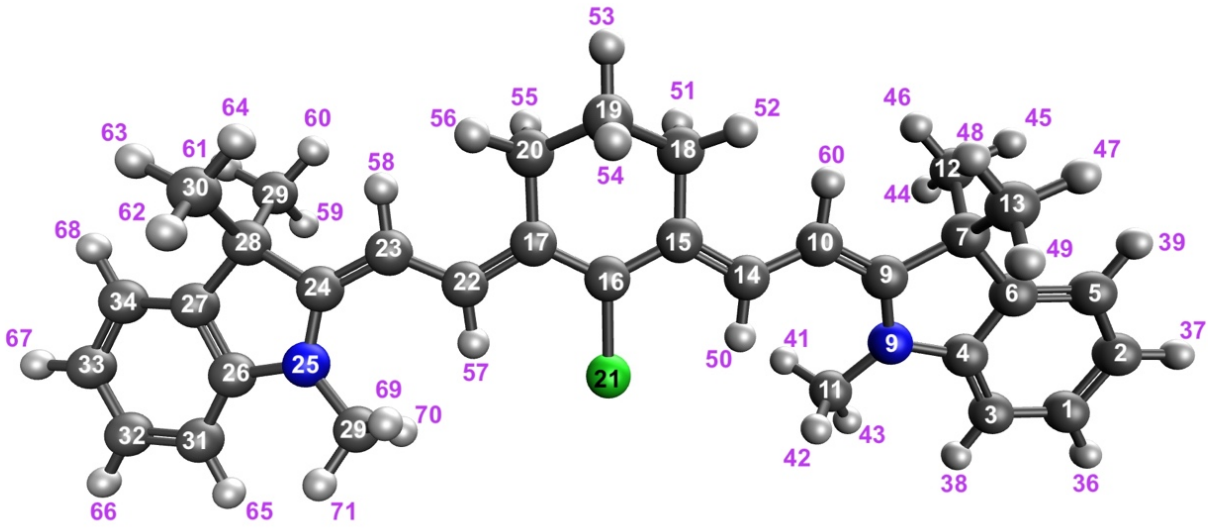

Figure S8. Chemical structure of IR-775 with geometry optimized at B3LYP/6-31++G(d,p).

Table S2. Comparison of the experimental and calculated (B3LYP/6-311++G(d,p))[a] Raman spectra of IR-775 (Figure S4) in spectral range 200 – 2000 cm^{-1}.

Raman Shift, cm^{-1}		Assignments[b]
Experimental	Calculated[b]	
516	528	$\omega(C_{17}–C_{16}–C_{15})$, $\omega(H_{53}–C_{19}–C_{54})$
563	570	$\gamma(C_{24}–C_{28}–C_{29})$, $\gamma(C_{8}–C_{7}–C_{12})$
792	774	$\omega(H_{62}–C_{30}–H_{64})$, $\omega(H_{48}–C_{13}–C_{49})$
928	939	$\gamma(C_{22}–H_{57})$, $\gamma(C_{14}–H_{50})$
1118	1125	$\omega(H_{69}–C_{35}–H_{70})$, $\omega(H_{42}–C_{11}–C_{43})$
1231	1213	$\delta(C_{3}–H_{68})$, $\nu(C_{28}–C_{24})$, $\delta(C_{5}–H_{39})$, $\nu(C_{28}–C_{24})$
1358	1354	$\nu(C=C)_{benzene}$
1530	1544	$\nu(C_{22}–C_{17})$, $\nu(C_{15}–C_{14})$, $\nu(N_{9}–C_{8}–C_{10})$, $\nu(N_{25}–C_{24}–C_{23})$, $\delta(H_{70}–C_{35}–H_{71})$
1582	1608	$\nu(C_{34}–C_{27})$, $\nu(C_{32}–C_{31})$

[a] Empirically chosen scaling factor: 0.98.

[b] ν, stretch; δ, in-plane bend; γ, out-of-plane bend.

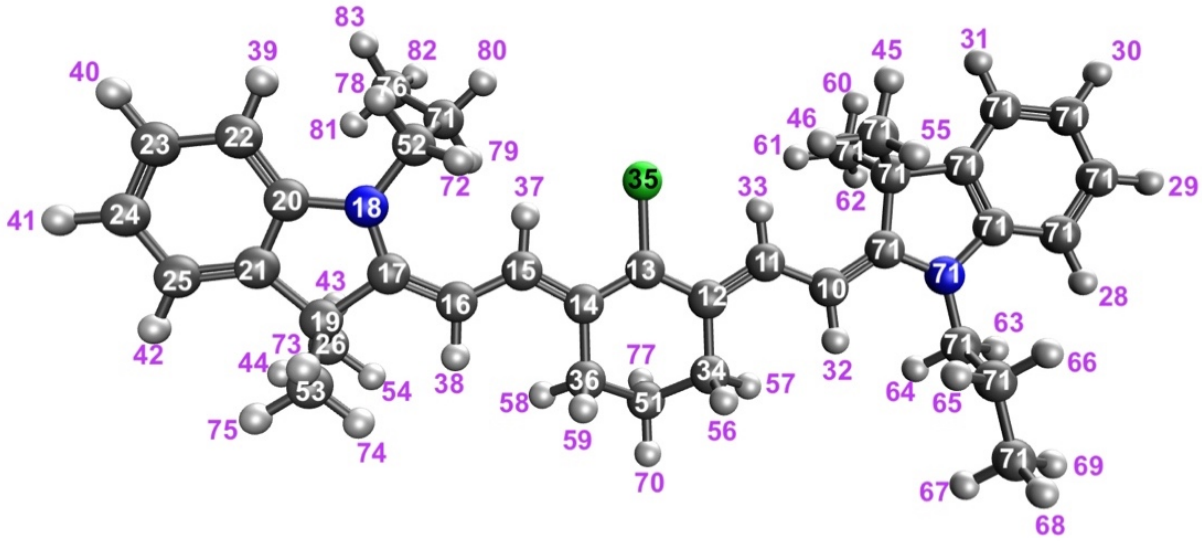

Figure S9. Chemical structure of IR-780 with geometry optimized at B3LYP/6-31++G(d,p).

Table S3. Comparison of the experimental and calculated (B3LYP/6-311++G(d,p))[a] Raman spectra of IR-780 (Figure S5) in spectral range 200 – 2000 cm^{-1}.

Raman Shift, cm^{-1}		Assignments[b]
Experimental	Calculated	
522	528	$\gamma(C_{14}–C_{13}–C_{12})$,$\delta(H_{58}–C_{36}–H_{59})$, $\delta(H_{70}–C_{51}–H_{77})$, $\delta(H_{56}–C_{34}–H_{57})$
557	548	$\delta(C_{53}–C_{19}–C_{26})$, $\delta(C_{27}–C_{9}–C_{47})$
1120	1122	$\delta(C–H)_{benzene\ ring}$
1205	1201	$\delta(C–H)_{cyclohexane\ ring}$
1368	1414	$\delta(C_{16}–H_{38})$, $\delta(C_{10}–H_{32})$, $\nu(C_{14}–C_{15})$
1465	1465	$\delta(H_{79}–C_{71}–H_{79})$, $\delta(C_{23}–C_{40})$, $\delta(C_{24}–H_{41})$
1525	1536	$\nu(N_{18}–C_{17}–C_{16})$, $\nu(C_{10}–C_{8}–N_{7})$, $\delta(H_{78}–C_{52}–H_{72})$
1583	1604	$\nu(C–C)_{benzene\ ring}$, $\delta(C–H)_{benzene\ ring}$

[a] Empirically chosen scaling factor: 0.98.

[b] ν, stretch; δ, in-plane bend; γ, out-of-plane bend.

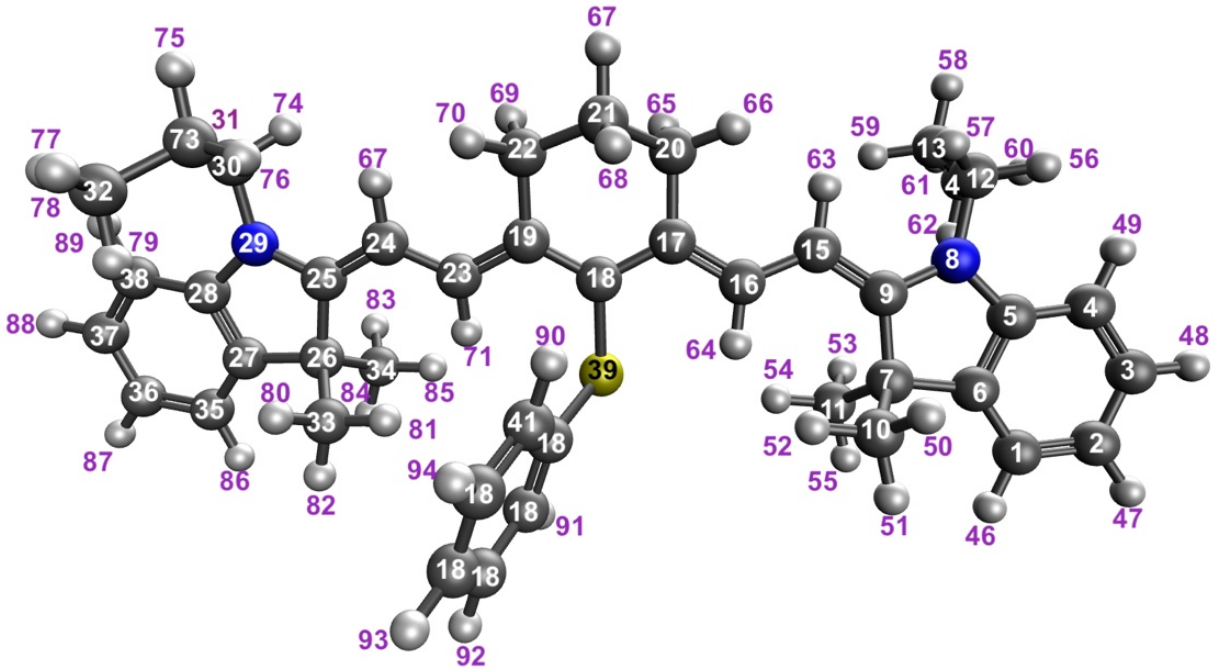

Figure S11. Chemical structure of IR-792 with geometry optimized at B3LYP/6-31++G(d,p).

Table S4. Comparison of the experimental and calculated (B3LYP/6-311++G(d,p))[a] Raman spectra of IR-792 (Figure S6) in spectral range 200 – 2000 cm^{-1}.

Raman Shift, cm^{-1}		Assignments[b]
Experimental	Calculated	
523	526	$\omega(H_{84}–C_{34}–H_{83})$, $\omega(H_{51}–C_{10}–C_{52})$
557	550	$\nu(S_{39}–C_{18})$, $\delta(C_{22}–C_{21}–C_{20})$
801	780	$\delta(C_{21}–H_{68})$, $\delta(C_{32}–H_{79})$, $\delta(C_{14}–H_{62})$
936	934	$\gamma(C–H)_{ring}$
1004	1025	$\nu(C_2–C_3)$, $\delta(C_1–H_{46})$, $\delta(C_4–H_{49})$
1206	1251	$\delta(H_{73}–C_{30}–H_{74})$, $\delta(H_{73}–C_{30}–H_{74})$, $\nu(C_{27}–C_{26}–C_{25})$, $\nu(C_9–C_7–C_6)$
1370	1355	$\delta(H_{73}–C_{30}–H_{74})$, $\delta(C_{31}–H_{76})$
1406	1392	$\delta(H_{78}–C_{32}–H_{79})$, $\nu(C_{19}–C_{18}–C_{17})$
1465	1466	$\delta(H_{69}–C_{22}–H_{70})$, $\delta(H_{65}–C_{20}–H_{66})$
1521	1530	$\nu(C_{25}–C_{24})$, $\nu(C_{23}–C_{19})$, $\nu(C_{17}–C_{16})$, $\nu(C_{15}–C_9)$, $\delta(C_{30}–H_{73})$, $\delta(C_{12}–H_{56})$
1581	1605	$\nu(C–C)_{ring}$

[a] Empirically chosen scaling factor: 0.98.

[b] ν, stretch; δ, in-plane bend; γ, out-of-plane bend.

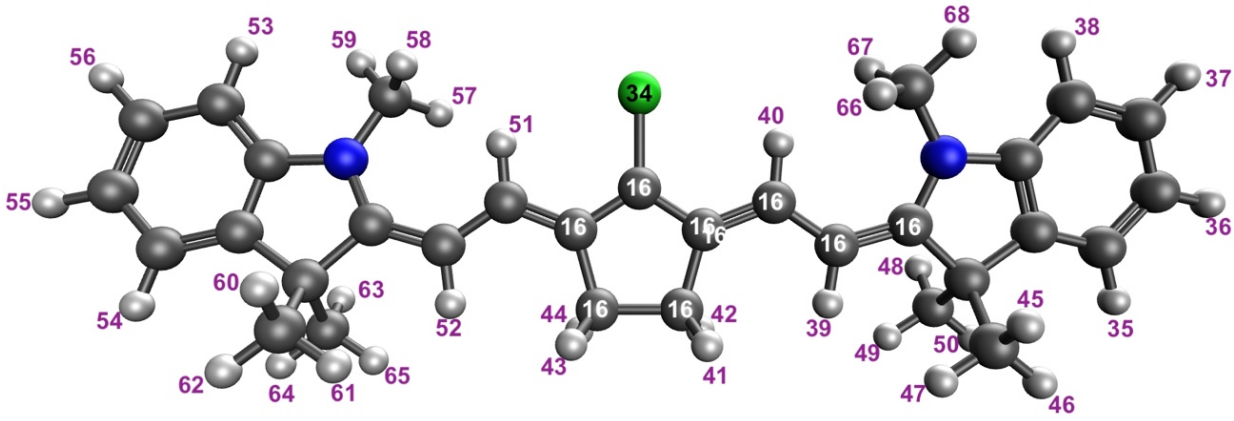

Figure S12. Chemical structure of IR-797 with geometry optimized at B3LYP/6-31++G(d,p).

Table S5. Comparison of the experimental and calculated (B3LYP/6-311++G(d,p))[a] Raman spectra of IR-797 (Figure S7) in spectral range 200 – 2000 cm^{-1}.

Raman Shift, cm^{-1}		Assignments[b]
Experimental	Calculated	
516	516	$\delta(C_6–C_5–C_4)$, $\delta(C_3–C_1–C_2)$, $\delta(C_{29}–C_{26}–C_{24})$, $\delta(C_{28}–C_{27}–C_{25})$
562	563	$\delta(C_{32}–C_{22}–C_{31})$, $\delta(C_{18}–C_7–C_{17})$
927	925	$\gamma(C_{20}–H_{50})$, $\gamma(C_{19}–H_{51})$, $\gamma(C_{11}–H_{40})$, $\gamma(C_{10}–H_{39})$
1038	1028	$\delta(C_{27}–H_{54})$, $\delta(C_4–H_{35})$, $\nu(C_{28}–C_{29})$, $\nu(C_5–H_4)$
1122	1124	$\delta(C_{28}–H_{55})$, $\delta(C_{29}–H_{56})$, $\delta(C_{26}–H_{53})$, $\delta(C_5–H_{38})$, $\delta(C_4–H_{37})$, $\delta(C_2–H_{36})$
1230	1276	$\delta(C_{19}–H_{51})$, $\delta(C_{11}–H_{40})$
1363	1353	$\nu(C–C)_{ring}$, $\nu(C_{15}–C_{16}–C_{12})$
1438	1454	$\delta(C_{20}–H_{52})$, $\delta(C_{10}–H_{39})$, $\delta(H_{58}–C_{30}–H_{59})$, $\delta(H_{66}–C_{33}–H_{68})$, cyclopentene breathing
1551	1561	$\nu(C_{21}–C_{20})$, $\nu(C_{10}–C_8)$, cyclopentene breathing
1609	1608	$\nu(C_{28}–C_{29})$, $\nu(C_{24}–C_{25})$, $\nu(C_3–C_6)$, $\nu(C_2–C_4)$

[a] Empirically chosen scaling factor: 0.98.

[b] ν, stretch; δ, in-plane bend

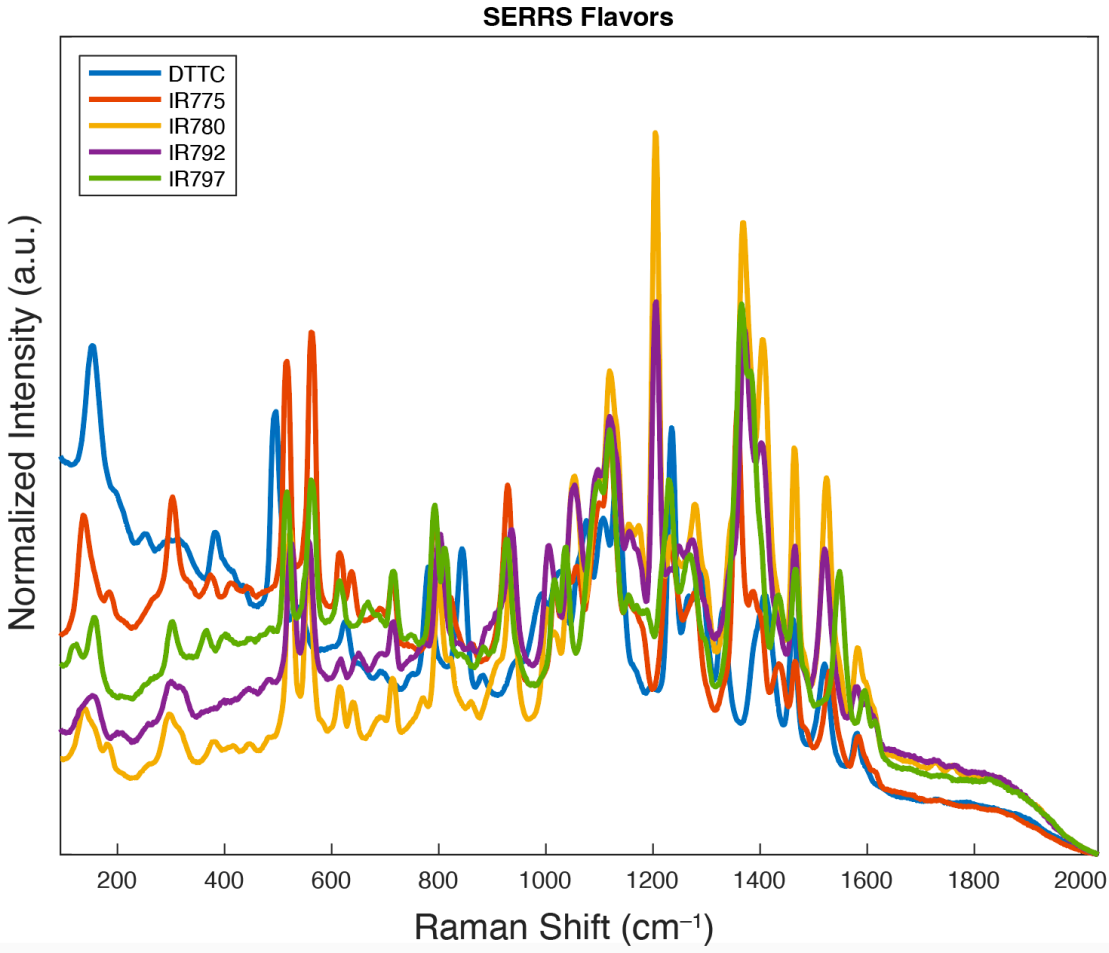

Figure S13. SERRS spectra of AuNPs labeled with DTTC, IR-775, IR-780, IR-792, and IR-797 acquired with 785 nm excitation wavelength, shown with no baseline subtraction.

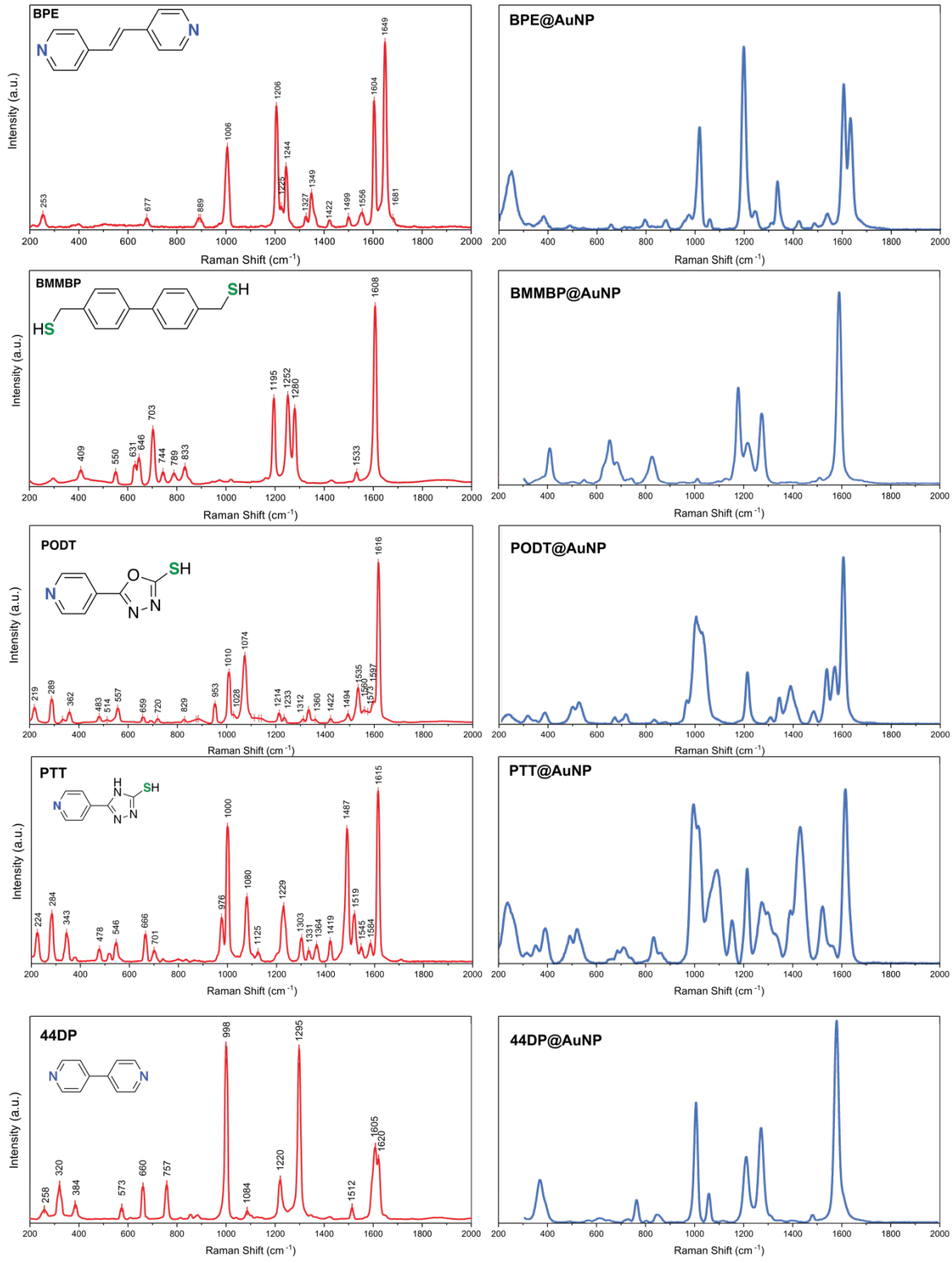

Figure S14. Normal Raman spectra of *trans*-bis(4-pyridyl)ethylene (BPE), 4,4′-bis(mercaptomethyl)biphenyl (BMMBP), 5-(4-pyridyl)-1,3,4-oxadiazole-2-thiol (PODT), 5-(4-pyridyl)-1H-1,2,4-triazole-3-thiol (PTT), and 4,4′-dipyridyl (44DP) measured from purified crystalline powder using 785 nm excitation wavelength (red). SERS spectra of AuNPs labeled with BPE, BMMBP, PODT, PTT, and 44DP using 785 nm excitation wavelength (blue), with no baseline subtraction.

Table S6. Correlation matrix built from the Raman spectra of SERS NPs. The correlation was calculated as a spectral inner product between all possible 2-plex combinations of the non-resonant Raman reporters among five SERS NP flavors. The correlation values indicate the level of overlapping signals, where 1 means 100% overlap and 0 means 0% overlap.

	BPE	**BMMBP**	**PODT**	**PTT**	**44DP**
BPE	1.00	0.63	0.71	0.59	0.67
BMMBP	0.63	1.00	0.66	0.58	0.79
PODT	0.71	0.66	1.00	0.72	0.78
PTT	0.59	0.58	0.72	1.00	0.68
44DP	0.67	0.79	0.78	0.68	1.00

Table S7. Correlation matrix built from the Raman spectra of SERRS NPs. The correlation was calculated as a spectral inner product between all possible 2-plex combinations of the NIR dyes among five SERRS NP flavors. The correlation values indicate the level of overlapping signals, where 1 means 100% overlap and 0 means 0% overlap.

	DTTC	**IR-775**	**IR-780**	**IR-792**	**IR-797**
DTTC	1.00	0.95	0.80	0.87	0.90
IR-775	0.95	1.00	0.86	0.92	0.97
IR-780	0.80	0.86	1.00	0.98	0.93
IR-792	0.87	0.92	0.98	1.00	0.97
IR-797	0.90	0.97	0.93	0.97	1.00

Table S8. Lowest and highest condition numbers (CNs) for ill-conditioned and well-conditioned, respectively, subsets of SERS and SERRS NPs without baseline subtraction

Number of	Lowest CN		Highest CN		Well-conditioned NP subset	
NP flavors	SERS	SERRS	SERS	SERRS	SERS	SERRS
1	1	1	1	1	-	-
2	2.29	3.29	3.39	14.26	BPE, PODT	IR780, DTTC
3	3.43	7.69	4.38	34.95	BPE, BMMBP, PODT	IR780, DTTC, IR775
4	4.64	32.31	5.28	42.90	BPE, BMMBP, PODT, PTT	IR780, DTTC, IR775, IR797
5	5.80	47.49	5.80	47.49	BPE, BMMBP, PODT, PTT, 44DP	IR780, DTTC, IR775, IR797, IR792

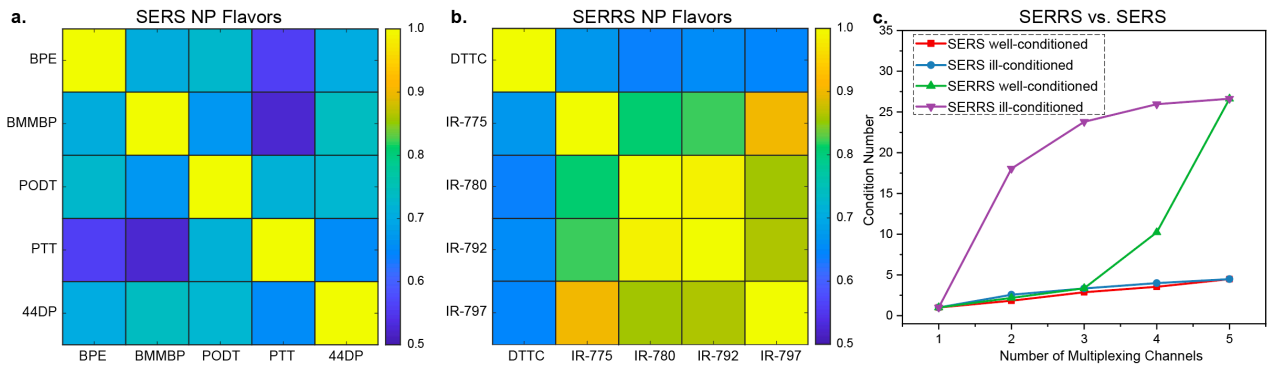

Figure S15. Multiplexing compatibility of SERS and SERRS NPs calculated based on the individual **baseline-subtracted reference spectra**. (a) Correlation matrices built from the spectra of SERS NPs (a) and SERRS NPs (b) demonstrating similarity among each type of flavors. The color bar indicates the level of fitting signals, where 1 (yellow) means 100% spectral overlap of two flavors and 0 (dark blue) means 50% spectral overlap of two flavors. (c) The lowest (well-conditioned subsets) and the highest (ill-conditioned subsets) condition numbers for different plexity of SERS and SERRS NP flavors (see Supplementary Information Table S8). A lower condition number is preferred to achieve easier unmixing of the NP subsets and higher plexity imaging. Notice how both the ill- and well-conditioned subsets of NP mixtures maintain a low condition number for the SERS NPs as opposed to the SERRS NPs. For deriving the condition number for each combination, we used the normalized reference spectra of SERS and SERRS NPs without baseline subtraction.

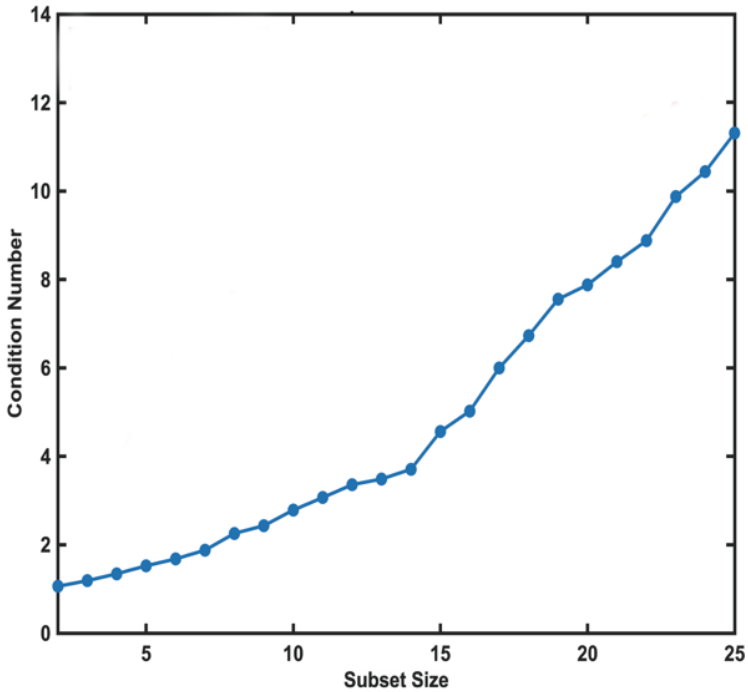

Figure S16. The lowest condition numbers for well-conditioned subsets of different plexity of SERS NP among 26 flavors reported by our group previously.[1] For deriving the condition number for each combination, we used the normalized reference spectra of SERS NPs.

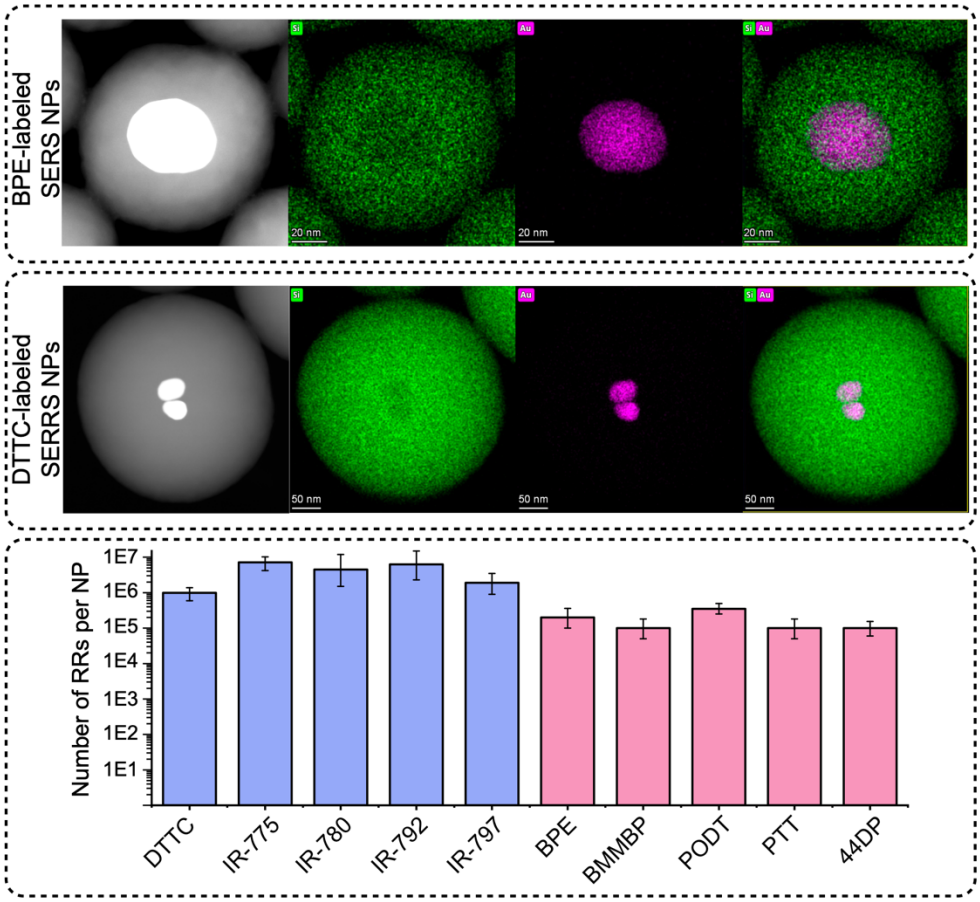

Figure S17. TEM images of BPE- and DTTC-labeled nanoparticles with EDS channels for Au (magenta) and Si (green). Average number of Raman reporter (RR) molecules per AuNP core for each spectral flavor.

Figure S18. Concentrations of SERS and SERRS nanoparticle colloidal solutions applied onto the filter paper substrate for dilution series.

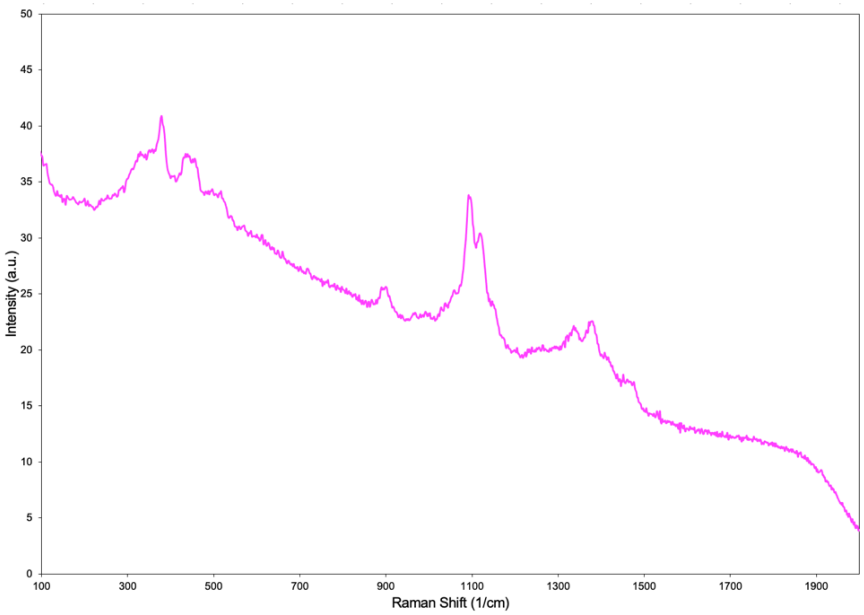

Figure S19. Average Raman spectrum of the paper substrate background (at λ_{ex} 785 nm, 0.1 s acquisition time, 2.5% neutral density filter used for all measurements, n = 500).

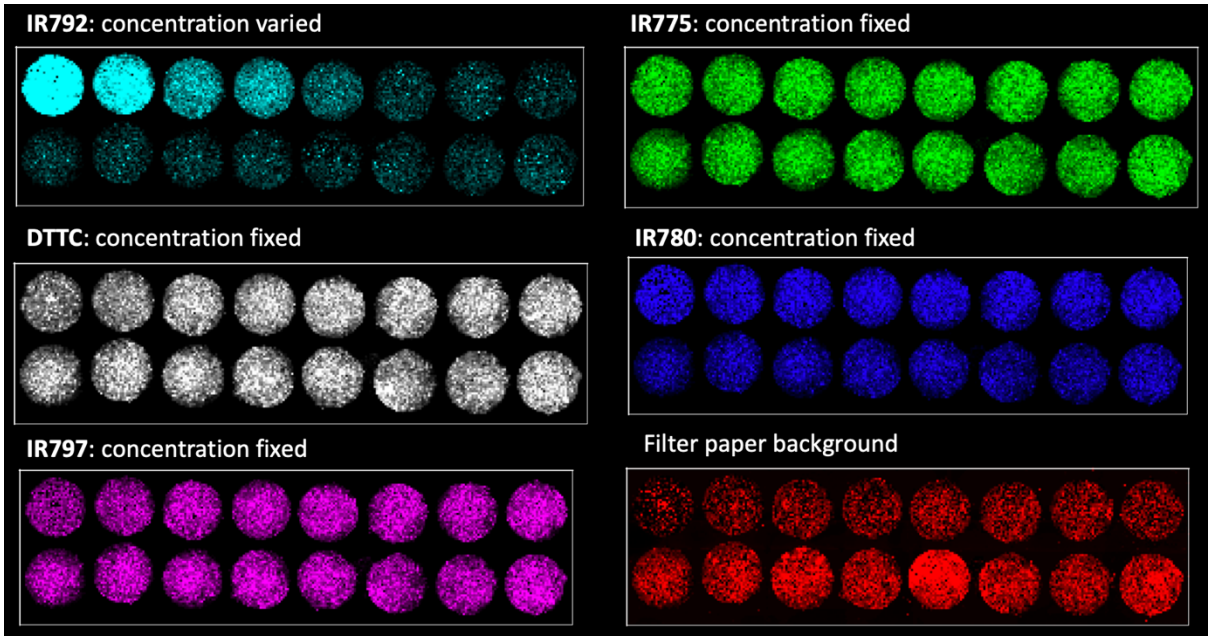

Figure S20. Unmixed weight values for SERRS NPs in 5-plex mixtures from a single image acquisition where the IR-792 concentration was diluted from 150 pM with 2-fold dilutions (as shown in Figure 4c) and concentrations of all other four SERRS NPs kept at 37.5 pM.

Table S10. Assignments of experimental Raman and SERS spectra for BPE, BMMBP, PODT, PTT,[2] and 44DP.

Raman		SERS		Assignments
Raman Shift, cm^{-1}	Normalized Intensity, a.u.	Raman Shift, cm^{-1}	Normalized Intensity, a.u.	
BPE – C_{2h} symmetry				
1006	0.436	1023	0.511	ring breathing
1206	0.655	1203	1.000	ν(ring–C_{vin}), δ(C–H)$_{py}$
1244	0.330	1251	0.121	δ(C–H)$_{vin}$, in-plane ν_{ring}
1349	0.187	1339	0.303	δ(C–H), δ(C_{vin}–C)
1604	0.684	1610	0.943	ν(C–C)$_{py}$, δ(C–H)$_{py}$
1649	1.000	1638	0.724	ν(C=C)$_{vin}$
BMMBP – C_2 symmetry				
1195	0.485	1189	0.515	δ(C–H)
1252	0.503	1225	0.226	$\gamma_s(CH_2)$
1280	0.428	1286	0.371	inter-ring C–C stretching, δ_{as}(C–H)$_{bp}$
1608	1.000	1606	1.000	ν(C–C)$_{bp}$, δ(C–H)$_{bp}$
PODT – C_s symmetry				
953	0.121	–	–	ν(N–N)$_{ox}$, ν(C–O)$_{ox}$, δ(S–H), (ring breathing)$_{py}$
1010	0.318	998	0.694	ν(N–N)$_{ox}$, ν(C–O)$_{ox}$, ν(C–S)$_{ox}$, (ring breathing)$_{py}$
1074	0.423	–	–	δ(C–H)$_{py}$
1535	0.222	1540	0.326	ν_s(C–N)$_{ox}$, $\nu_{py\ ring}$, ν(C_{py}–C_{ox}), δ_{as}(C–H)$_{py}$
1560	0.082	1571	0.345	ν(C=N)$_{tr}$, ν(C–C)$_{py}$, ν(C–N)$_{py}$
1616	1.000	1606	1.000	ν_s(C–C)$_{py}$, δ_s(C–H)$_{py}$
PTT – C_s symmetry				
1000	0.793	994	0.521	δ(N–C–N)$_{py}$, δ(C–N–C)$_{py}$, δ(C–C–C)$_{tr}$, ν(N–C)$_{tr}$
1080	0.381	1094	0.423	δ(H–C–C), δ(C–C–N)
1229	0.327	1210	0.421	δ(H–C–N)$_{py}$, δ(H–C–C)$_{py}$, ν(N–C)$_{py}$
1487	0.779	1431	0.751	ν(N–C)$_{tr}$
1615	1.000	1611	1.000	ν(C–C)$_{py}$, δ(H–C–C)$_{py}$
44DP – C_{2v} symmetry				
998	1.000	1000	0.596	(ring breathing)$_{py}$
1102	0.022	1073	0.145	δ(C–H)$_{asym}$
1220	0.228	1231	0.327	δ(C–H)$_{sym}$
1295	0.983	1293	0.469	ν(C–C)$_{et}$
1606	0.417	1609	1.000	ν(C=C)$_{py}$
1620	0.350			ν(C=C)$_{py}$

REFERENCES

1. Eremina, O. E.; Czaja, A. T.; Fernando, A.; Aron, A.; Eremin, D. B.; Zavaleta, C., Expanding the Multiplexing Capabilities of Raman Imaging to Reveal Highly Specific Molecular Expression and Enable Spatial Profiling. *ACS Nano* **2022,** *16* (7), 10341-10353.
2. Eremina, O. E.; Eremin, D. B.; Czaja, A.; Zavaleta, C., Selecting Surface-Enhanced Raman Spectroscopy Flavors for Multiplexed Imaging Applications: Beyond the Experiment. *J. Phys. Chem. Lett.* **2021,** *12* (23), 5564-5570.